ACADÉMIE
DES SCIENCES
INSTITUT DE FRANCE

Comptes Rendus
Chimie

Jingdi Zheng, Shuang Tao, Ying Yang and Ying Tang

Gel–sol synthesis of hierarchical CaO using pollen as biotemplate for biodiesel production

Volume 27, Special Issue S3 (2024), p. 129-142

Online since: 14 May 2024

Part of Special Issue: Materials and Energy Valorization of Biomass and Waste: The Path for Sustainability and Circular Economy Promotion

Guest editors: Mejdi Jeguirim (Université de Haute-Alsace, Institut de Sciences des Matériaux de Mulhouse, France) and Salah Jellali (Sultan Qaboos University, Oman)

https://doi.org/10.5802/crchim.269

The Comptes Rendus. Chimie *are a member of the Mersenne Center for open scientific publishing*
www.centre-mersenne.org — e-ISSN : 1878-1543

ACADÉMIE DES SCIENCES
INSTITUT DE FRANCE

Comptes Rendus. Chimie
2024, Vol. 27, Special issue S3, p. 129-142
https://doi.org/10.5802/crchim.269

Research article

Materials and Energy Valorization of Biomass and Waste: The Path for Sustainability and Circular Economy Promotion

Gel–sol synthesis of hierarchical CaO using pollen as biotemplate for biodiesel production

Jingdi Zheng [a], Shuang Tao [a], Ying Yang [a] and Ying Tang [*, a, b]

[a] Shaanxi Province Key Laboratory of Environmental Pollution Control and Reservoir Protection Technology of Oilfields, Xi'an Shiyou University, Xi'an, China

[b] Engineering Research Center of Oil and Gas Field Chemistry, Universities of Shaanxi Provence, Xi'an Shiyou University, Xi'an, China

E-mail: tangying78@xsyu.edu.cn (Y. Tang)

Abstract. In this paper, a novel hierarchical calcium-based catalyst marked as CaO(S) has been established to catalyze oil-methyl acetate-methanol for no-glycerol biodiesel production. The CaO(S) was synthesized through sol–gel-biotemplate method using calcium nitrate-ethanol-citric acid as precursor and rape pollen as biotemplate, followed by the characterizations such as N_2-Brunauer Emmet Teller (N_2-BET), X-ray diffraction (XRD), Fourier transform-infrared (FT-IR), CO_2-temperature programmed desorption (CO_2-TPD), Thermogravimetry differential thermal analysis (TG-DTA) and scanning electron microscopy (SEM). The results indicate that pollen as a biotemplate could be used to improve the basicity and textural parameters of calcium oxide particles, especially for 1/1-CaO(S)-700, presented by its total basicity of 5.90 mmol/g, the specific surface area of 16.47 m^2/g, the pore volume of 0.04 cm^3/g, the average pore size of 10.28 nm, and the widespread distribution of pore size (2–12.5 nm). Moreover, the yield of no-glycerol biodiesel, 96.62%, has been investigated after 3 h under optimized conditions (temperature = 65 °C, dosage of CaO(S) = 10 wt%, oil/methyl acetate/methanol = 1/1/8), by the yield presence of 91.37% after 3 cycles, which indicated that the 1/1-CaO(S)-700 prepared by sol–gel-biotemplate method had good stability.

Keywords. Biodiesel, Rape pollen, Sol–gel method, Tri-component coupling transesterification, CaO.

Funding. National Natural Science Foundation of China (No. 51974252) and Youth Innovation Team of Shaanxi University, Xi'an Shiyou University Graduate Innovation Project (YCS22213106).

Manuscript received 5 May 2023, revised 2 September 2023 and 24 October 2023, accepted 24 October 2023.

1. Introduction

Energy as the backbone of the country's future development, its industrialization and per capita consumption has become an important measure of human technology and living standards, especially in the rapid development of industrialization today [1]. The dieselization of vehicles is a major driving force for the reform of the fuel market, which makes the promotion and development of the diesel industry become the focus of public attention [2]. It can be observed that petrochemical diesel is mainly a derivative from crude oil after a series of processes such as distillation, catalytic cracking, thermal cracking, hydrocracking, and petroleum coking, and most of them are hydrocarbons [3]. However, petrochemical diesel has two major constraints of high sulfur

* Corresponding author

and high nitrogen contents, which have seriously shaken the ecological civilization, typically of the atmospheric environment [4]. As a model of biomass energy, biodiesel has dual benefits, which can not only avoid price fluctuations caused by traditional non-renewable fuels, but also achieve structural energy conservation and emission reduction [5]. At present, the most mature theory of biodiesel is based on the development of oil (Triglycerides, TG) and low-chain alcohol (Methanol, MeOH) into generate biodiesel (Fatty Acid Methyl Ester, FAME) with carbon chain lengths ranging from 16 to 20 [6]. The oil–alcohol transesterification with the participation of base catalyst will generate a large amount of glycerol, among which, there is 1/10 of glycerol in every 10 t of methyl ester fuel, affecting its combustion performance and low temperature flow, and even the operation of diesel engines [7]. Methyl acetate (MeOAc), an organic acid that is miscible with alcohol, is often used as an acetylating solvent to react with glycerol to prepare glycerol acetate [8]. Therefore, the introduction of methyl ester reagent in oil–alcohol not only achieves the in situ conversion of glycerol, but also improves its performance.

Calcium oxide material, as one of the conventional heterogeneous catalysts, is an oxide composed of divalent oxygen anion and the most active divalent calcium ion in alkaline earth metals, most of which are prepared by calcinating calcium-containing minerals, mollusk shells, eggshells, and bones, etc [9]. The melting temperature of CaO is 2572 °C, and its ionic spacing and crystal structure is similar to NaCl, which belongs to a typical ionic crystal with cubic structure. Among them, calcium ions and two adjacent oxygen ions are cross-linked through electrostatic attraction and three-dimensionally extended into a cubic structure [10]. Wang et al. used modified CaO by bromobenzene to catalyze the Aldol reaction (acetophenone–benzaldehyde) to generate chalcone with the yield of 98.9%, and also proved that the Aldol reaction was performed by Ca^{2+} activated the carbonyl group of acetophenone and O^{2-} activated the aldehyde group of benzaldehyde [11]. Subsequently, the CaO as a catalyst was added in a mixed solution of glycerol-dimethyl carbonate (1/2) so as to investigate the mechanistic pathways to the formation of glycerol carbonate, as studied by Simanjuntak et al. [12]. Besides, CaO is also widely involved in transesterification reactions. Leandro et al. investigated the catalytic ability of natural waste biomass calcium oxide (crab shell and egg shell) after calcinating. It is found that the resulting nano-CaO materials play an important role in the transformation of FAME from TG and MeOH, which presents the yields of FAME are 83.10 ± 0.27 wt% and 97.75 ± 0.02 wt%, respectively [13]. Thus, CaO is a valuable and promising solid base catalyst, which is widely used in various organic reactions. However, commercial calcium oxide is almost obtained by calcining limestone, resulting in poor dispersibility and poor internal pore structure [14]. Therefore, an increasing number of researchers have gradually shifted their study focus to the synthesis and application of highly dispersed metal oxide with hierarchical structure, in order to solve the defects of traditional calcium oxide.

The addition of template can regulate the morphology, structure and even dispersion, so as to further achieve the purpose of improving its catalytic properties. It is necessary initially to classify the templates into certain types, such as physical, chemical, and biological template [15]. Li et al. synthesized three kinds of CaO-based sorbents using $Ca(CH_3COO)_2$, $Ca(OH)_2$ and $CaCO_3$ as precursors by a wet mixing method with the help of aluminate cement and organic fiber, and the cyclic performance of the sorbent decomposed from $Ca(CH_3COO)_2$ is better. It also verifies that it plays an important role in CO_2 capture [16]. It is secondary that there are abundant biological templates, which can quickly and controllably prepare many metal oxides with different compositions and biological forms. The most typical ones are yeast, cotton, wood, filter paper, jute fiber, pomelo, birch, rice, pollen, etc. [17–25]. Rape pollen, with a special network structure and three-dimensional pores, is of great inspiration for the preparation of highly dispersed solid bases, and there are a certain number of hydroxyl and carboxyl groups on its surface, which helps the metal ions diffuse to the surface uniformly, thereby forming nucleation sites for further meristems and assembly [26].

This study aims to investigate the gel–sol synthesis of hierarchical CaO using pollen as a template and calcium nitrate-ethanol-citric acid as precursor. The application of the derived CaO(S) in catalytic oil-methyl acetate-methanol production of no-glycerol biodiesel was studied. The CaO(S)-based catalysts

were characterized and analyzed to elucidate the effects of their preparation conditions on pore structure, basicity, and dispersion and their relationship to catalytic performance.

2. Experimental details

2.1. *Reagents*

The required analytical reagents, namely methyl acetate ($C_3H_6O_2$, Kelon Co.), anhydrous methanol (CH_3OH, Fuyu Co.), sodium hydroxide (NaOH, Tianli Co.), cyclohexane (C_6H_{12}, Tianli Co.), methyl heptadecanoate ($C_{18}H_{38}O_2$, TCI Co.), anhydrous ethanol (C_2H_5OH, Fuyu Co.), calcium nitrate tetrahydrate ($Ca(NO_3)_2{\cdot}4H_2O$, Damao Co.), citric acid ($C_6H_8O_7{\cdot}H_2O$, Kelon Co.), were purchased from China. The rapeseed oil was obtained from Shanxi Jianxing Co., China. The rape pollen broken at ultra-low temperature was obtained from Henan Changge Yanyuan Bee Products Co., China.

2.2. *Characterization techniques*

The textural properties of CaO(S) were determined by Micromeritics ASAP 2020 HD88 (Norcross, Georgia, USA) [27]. The crystalline structures of CaO(S) were identified by D8 ADVAHCL (Germany) (Cu-Kα, λ = 1.5406 Å) with a scan voltage of 40 kV, a current of 30 mA and a 2θ range of 10°–80° [28]. The FT-IR spectras of CaO(S) were recorded by Nicolet 5700 (Madison, Wisconsin, USA) in the wavenumber ranging from 4000 to 400 cm^{-1} [29]. The thermogravimetric experiments of CaO(S) were performed by TGA-SDTA851 analyzer (Shanghai, China) in a temperature range of 25–800 °C at a rate of 10 °C/min with a nitrogen flow rate of 50 mL/min [30]. The CO_2-TPD curves and its total basicity of CaO(S) were obtained by ChemiSorb 2750 (Norcross, Georgia, USA) and the morphology of CaO(S) was determined by JSM-6390A (Japan) [31,32].

2.3. *Gel–sol synthesis of hierarchical CaO*

An ethanol solution of a predetermined concentration of calcium nitrate tetrahydrate ($Ca(NO_3)_2{\cdot}4H_2O$) with 1 mol/L, denoted by CN, as a Ca^{2+} precursor and porous template (rape pollen after ultrasonic cleaning with ethanol) were magnetically stirred in a water bath at 30 °C, followed by the addition of citric acid (CA) and stirring at 70 °C for 3 h to form gels based on the pollen skeleton. The solutions with three different molar ratios of CN to CA from 1/0.5 to 1/1.5, denoted at X-CaO(S) where X is the CN/CA ratio, S is the sol–gel method containing different citric acid concentrations of 0.5 mol/L, 1 mol/L and 1.5 mol/L were prepared and then centrifuged and dried, finally calcined to obtain powder. The calcination conditions of the muffle furnace (KFS-7-12, Shanghai) were a calcination temperature in range of 600–800 °C, a calcination time of 3 h under an air atmosphere. Target sample CaO was obtained, denoted X-CaO(S)-Y, Y represents the calcination temperature. Schematic diagram of the specific preparation process of CaO(S) by sol–gel method is shown in Figure 1. The synthetic reactions are shown in Equations (1)–(5). Commercial CaO (Kelon Co.), used as a benchmark, was calcined at 700 °C under an air atmosphere for 3 h (denoted as Commercial CaO-700).

$$Ca^{2+} + 2C_6H_7O_7^- \rightarrow Ca(C_6H_7O_7)_2 \quad (1)$$

$$Ca(C_6H_7O_7)_2 + OH^- \rightarrow Ca(OH)(C_6H_7O_7) + C_6H_7O_7^- \quad (2)$$

$$Ca(OH)(C_6H_7O_7) + OH^- \rightarrow Ca(OH)_2 + C_6H_7O_7^- \quad (3)$$

$$Ca(OH)_2 + Ca(OH)_2 \rightarrow Ca-O-Ca-O + 2H_2O \quad (4)$$

$$Ca(OH)_2 \rightarrow CaO + H_2O\uparrow \quad (5)$$

2.4. *Preparation of no-glycerol biodiesel*

The refining process of rapeseed oil was carried out in a beaker with a mass ratio of oil and lye (1 mol/L NaOH) of 4:1 or 5:1, in order to avoid the catalytic performance of free fatty acids in oil to solid base. Therefore, the raw oil should be reacted with the lye under magnetic stirring for 5 h, and then washed with boiled water and separated in a separatory funnel until the pH of the lower water was about 7.0, followed by the addition of quantitative cyclohexane. It was dehydrated in a device equipped with a water separator and a reflux condenser, and finally the excess cyclohexane was removed by using a rotary evaporator so as to purify oil.

To investigate the catalytic performance of CaO (S), the no-glycerol biodiesel generated from the tri-component coupling transesterification reaction was used as the target product, typically of synthesis in a 250 mL three-neck round bottom flask

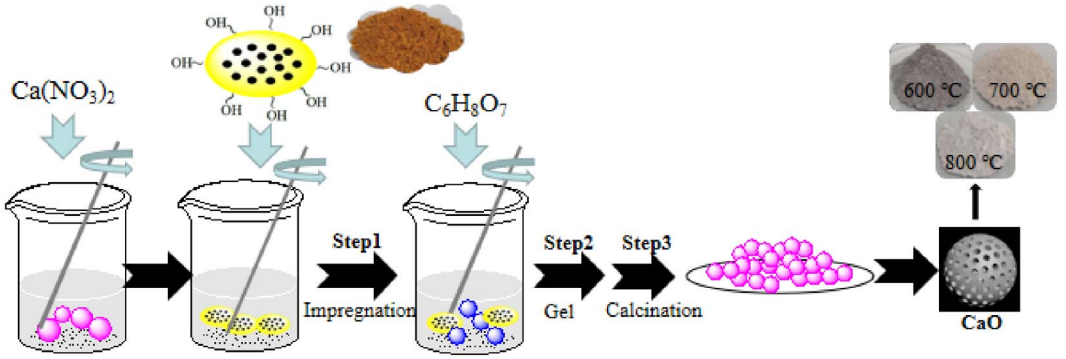

Figure 1. Schematic diagram of CaO(S) by sol–gel method.

equipped with a reflux condenser. A certain amount of CaO (S) was added to a mixed solution consisting of oil-methanol-methyl acetate, and the water bath temperature was controlled at 65 °C for 3.5 h. Subsequently, the biodiesel was collected every 20 or 30 min by centrifugation (4000 rpm, 30 min) and vacuum rotation evaporation (85 °C, 5 min) to remove solid CaO(S), unreacted methanol (boiling point: 64.5 °C) and methyl acetate (boiling point: 57.8 °C).

A quantitative analysis of biodiesel (FAME) was performed by gas chromatography (Yiyou-GC7860, N_2 as carrier gas, FID detector, KB-Wax capillary column) based on internal standard method (methyl heptadecanoate as internal standard, cyclohexane as solvent). The oven, injector, and detector temperatures were set to 100 °C, 250 °C, and 280 °C, respectively. The temperature program was divided into three stages, heating from 100 °C to 200 °C at 20 °C/min and holding for 3 min, then heating to 220 °C at 10 °C/min and keeping for 3 min, finally heating to 240 °C at 10 °C/min and staying for 3 min, among of which the entire analysis process lasted 20 min. The calculation formula of FAME yield is shown in Equation (6). $\sum A_i$, A_{MH} and C_{MH} are the peak areas of all FAMEs, the peak areas of methyl heptadecanoate and the concentration of methyl heptadecanoate (1 mg/mL). V_{MH} is the volume of internal standard solution (1 mL) and W is the net mass (mg) of the product.

$$\text{yield (\%)} = \left[\frac{(\sum A_i - A_{MH})}{A_{MH}}\right] \frac{C_{MH} V_{MH} \times 100}{W}. \quad (6)$$

3. Results and discussion

3.1. *Characterization of the CaO(S) catalyst*

3.1.1. *N_2-BET analysis*

Table 1 shows that when the calcination temperature is changed from 600 °C to 700 °C, the specific surface area of CaO(S) increases from 9.77 m^2/g to 16.47 m^2/g, and when the calcination temperature is further increased to 800 °C, the CaO(S) will be greatly reduced to 8.84 m^2/g, indicating that within the calcination temperature of CaO(S), an appropriate increase is beneficial to improve its pore structure. As shown in Figure 2(a), all CaO(S) have mesoporous structures (IV-type isotherm, H_3-type hysteresis loop) [33], and when the calcination temperature is 700 °C, the amount of nitrogen adsorption generated by 1/1-CaO(S)-700 is the largest at P/P_0 = 0–1, which includes the monolayer adsorption of nitrogen on the surface of CaO(S) ($P/P_0 < 0.4$) and the multimolecular adsorption of nitrogen ($P/P_0 > 0.4$) [34]. Besides, it is available from Figure 2(b), 1/1-CaO (S)-700 produces more mesopores with an average pore diameter concentrated at 3.5 nm and a relatively wide change (2–12.5 nm), indicating a hierarchical pore structure.

Table 2 shows the pore parameters of CaO(S) under different molar ratios of CN-CA, and Figure 3(a,b) is its N_2-adsorption–desorption isotherm and pore size distribution. It can be seen from Table 2 that when the molar ratio of CN-CA is changed from 1/0.5 to 1/1, the specific surface area of CaO(S) increases from 9.90 m^2/g to 16.47 m^2/g, and the pore volume

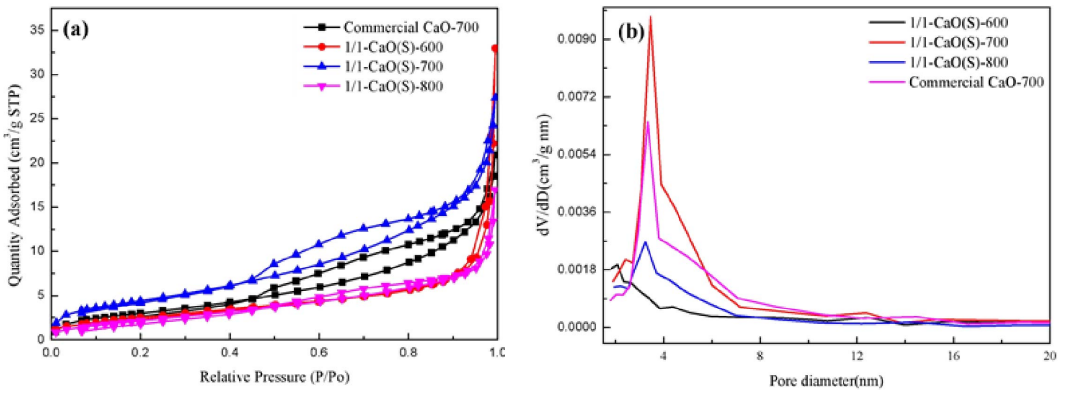

Figure 2. (a) N_2-adsorption–desorption isotherms and (b) pore size distribution curve of CaO(S) under different calcination condition.

Table 1. Pore structure properties of CaO(S) under different calcination conditions and commercial CaO

Type of catalyst	BET surface area (m^2/g)	Pore volume (cm^3/g)	Average pore diameter (nm)
1/1-CaO(S)-600	9.77	0.05	20.89
1/1-CaO(S)-700	16.47	0.04	10.28
1/1-CaO(S)-800	8.84	0.03	11.88
Commercial CaO-700	11.45	0.03	11.31

is given by 0.02 cm^3/g increased to 0.04 cm^3/g, and the average pore diameter increased from 9.16 nm to 10.28 nm, which is an attribute of citric acid by providing a large amount of H^+ in the ethanol solution, promoting the hydrolysis of calcium salts and the polycondensation so as to a preferred performance of the CaO(S) gel [35]. When the CN-CA ratio is further increased to 1/1.5, the specific surface area of CaO(S) decreases from 16.47 m^2/g to 11.29 m^2/g, and the average pore diameter increases from 10.28 nm to 14.70 nm, indicating that the excessive citric acid can reduce the specific surface area and the number of pores, which is not conducive to efficient diffusion of reactants of different sizes in heterogeneous reaction systems.

3.1.2. *XRD analysis*

In order to study the effects of calcination conditions and the molar ratio of CN-CA on the crystalline structures of CaO(S), X-ray scanning was performed to obtain its XRD patterns, as shown in Figure 4(a), which can enable a longitudinal comparison of the changes of the crystalline structures of the CaO(S) calcined at 600 °C, 700 °C and 800 °C, respectively. It can be seen that the calcination conditions are related to the phase composition, particle size and even the dispersion of CaO(S) particles. Among them, the diffraction peaks of 1/1-CaO(S)-600 at 2θ = 22.96°, 29.29°, 35.86°, 39.43°, 43.18°, 47.38°, and 48.48° match well with the standard card JCPDS 33-0268 classified as the typical calcite $CaCO_3$, which can be inferred that when the calcination temperature is 600 °C, the CaO crystals are not completely formed and mainly exist in the form of carbonate [36]. However, when the calcination temperature is further increased to 700 °C or 800 °C, the carbonate gradually decomposes to form calcium oxide, resulting in a more perfect crystal structure and an increase in particle size (Scherrer formula: $D = K\lambda/B\cos\theta$), which can be found in the crystal plane comparison of CaO (JCPDS 48-1467, 2θ = 32.21°, 37.36°, 53.86°, 64.19°and 67.38°) [37]. Notably, the 1/1-CaO(S)-800 has sharp low-angle peak at 2θ = 32.21°, 37.36°, which is consistent with the relatively poor particle dispersion caused by sintering of the surface of the CaO(S) particles.

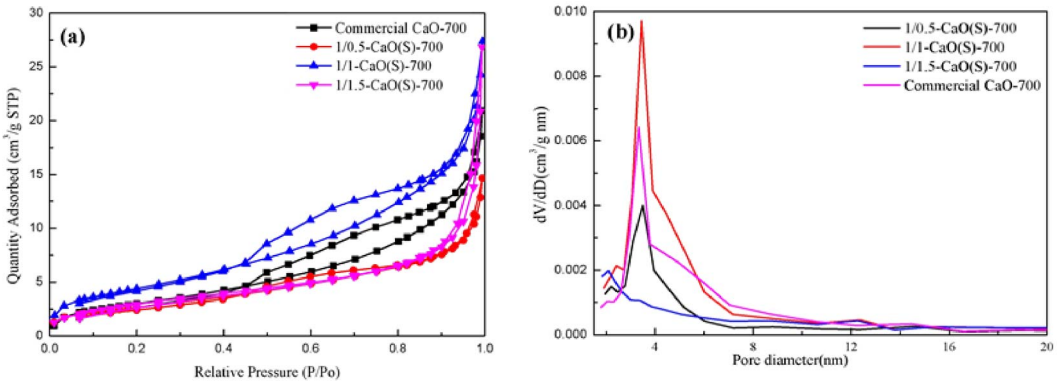

Figure 3. (a) N_2-adsorption–desorption isotherms and (b) pore size distribution curve of CaO(S) under different mole ratio of nitrate and citric acid.

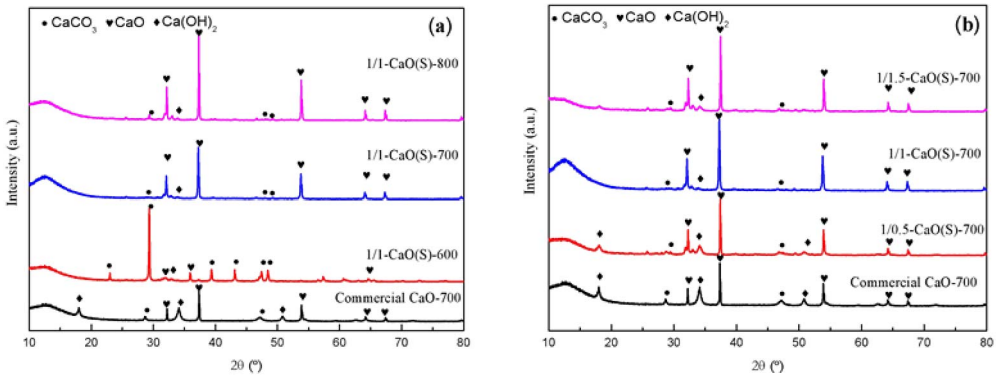

Figure 4. XRD patterns of the synthesized CaO(S) and Commercial CaO-700 (a) calcination conditions; (b) the mole ratio of nitrate and citric acid.

Table 2. Pore structure properties of CaO(S) under different mole ratio of CN-CA and commercial CaO

Type of catalyst	BET surface area (m^2/g)	Pore volume (cm^3/g)	Average pore diameter (nm)
1/0.5-CaO(S)-700	9.90	0.02	9.16
1/1-CaO(S)-700	16.47	0.04	10.28
1/1.5-CaO(S)-700	11.29	0.04	14.70
Commercial CaO-700	11.45	0.03	11.31

Figure 4(b) shows the XRD pattern of 1/0.5-CaO(S)-700, 1/1-CaO(S)-700, 1/1.5-CaO(S)-700 obtained from CN-CA solution at different molar ratios. It can be seen from Figure 4(b) that 1/0.5-CaO(S)-700 has a stronger CaO diffraction peak than Commercial CaO-700, and there are also miscellaneous peaks similar to $Ca(OH)_2$ and $CaCO_3$. When the amount of CA increases, the crystallinity and structural regularity of CaO in CaO(S) improve, which is attributed to the fact that CA not only adjusts the pH of the ethanol solution, but also reacts with calcium salts to form calcium citrate, resulting in avoiding the precipitation of calcium ions and promoting the hydrolysis of calcium salts and the polycondensation reaction. When the molar ratio of CN-CA is further increased to 1/1.5, the CaO peaks

of 1/1.5-CaO(S)-700 at 2θ = 32.21°, 37.36°, 53.86°, 64.19°, and 67.38° are stronger, suggesting a large particle size and poor dispersion [37].

3.1.3. *TG-DTA analysis*

TG-DTA analysis was performed on CaO(S) prepared at different calcination temperatures and impregnated with a 1/1 molar ratio of CN-CA, and the results are shown in Figure 5(a,b). According to Figure 5(a), the weight loss rates of $Ca(OH)_2$ (370–450 °C) and $CaCO_3$ (550–785 °C) in the presence of 1/1-CaO(S)-600 are 1.71% and 23.31% [38,39]. When the calcination temperature is 700 °C, 1/1-CaO(S)-700 has the weight loss rates of $Ca(OH)_2$ and $CaCO_3$ with 7.09% and 3.48%. Further increasing the calcination temperature to 800 °C, the weight loss of $Ca(OH)_2$ and $CaCO_3$ of CaO(S) are presented by 5.69% and 3.42%, implying that the erosion of CaO(S) is gradually weakened by CO_2 in the air, and the erosion of H_2O is gradually enhanced.

Figure 5(c–d) is the TG-DTA curves of CaO(S) prepared from CN-CA solutions with different molar ratios and calcinated at 700 °C. It is available from Figure 5(c), when the molar ratio of CN-CA is 1/0.5, the weight loss rates of $Ca(OH)_2$ (360–450 °C) and $CaCO_3$ (490–640 °C) corresponding to 1/0.5-CaO(S)-600 are 7.19% and 3.59% [38,39]. Further increasing the molar ratio of CN-CA to 1/1, the weight loss rates of $Ca(OH)_2$ and $CaCO_3$ derived from 1/1-CaO(S)-700 are 7.09% and 3.48%. When the molar ratio of CN-CA is 1/1.5, the weight loss rates of $Ca(OH)_2$ and $CaCO_3$ produced by 1/1.5-CaO(S)-700 are 4.10% and 3.07%, which shows that the erosion of CO_2 and H_2O on the CaO(S) surface is weakened as the CN-CA ratio changes from 1/0.5 to 1/1.5. It can be seen from Figure 5(d) that with the increase of the amount of CA, the endothermic peak temperature of $CaCO_3$ of CaO(S) is inclined to the direction of 800 °C, indicating that the thermal stability of the CaO(S) gel is improved. The decomposition temperatures of $Ca(OH)_2$ and $CaCO_3$ over the prepared CaO(S) are 400 °C and 613 °C, respectively, as shown in Figure 5(b), which are relatively lower than the results studies reported by Dj. Vujicic et al. [40] reflecting $Ca(OH)_2$ and $CaCO_3$ decomposition temperatures of 480 °C and 740 °C, respectively. Similar results has been found in previous research which indicated that low temperature decomposition usually related to higher dispersion [41].

3.1.4. *FT-IR analysis*

FT-IR analysis of CaO(S) from different calcination conditions was performed in the range of 4000–500 cm^{-1}. As shown in Figure 6(a), there are two types of functional groups are present, corresponding to the stretching vibration peaks of –OH (3648 cm^{-1}, 3448 cm^{-1} and 1647 cm^{-1}) and CO_3^{2-} (1459 cm^{-1}, 871 cm^{-1} and 713 cm^{-1}), respectively [42,43]. Compared with 1/1-CaO(S)-700 and 1/1-CaO(S)-800, the CO_3^{2-}-type peak of 1/1-CaO(S)-600 is relatively sharp, indicating that the main crystal composition is carbonate in the presence of 1/1-CaO(S)-600. When the calcination temperature increases from 600 °C to 800 °C, the stretching vibration peak of CO_3^{2-} gradually becomes weaker, and the peak of –OH gradually becomes sharper, indicating that the strong hydroxylation and weak carbonation of CaO(S) as the calcination temperature ranging from 600 °C to 800 °C, as described by TG-DTA analysis.

Figure 6(b) shows the FT-IR spectras of CaO(S) prepared from different CN-CA molar ratios under the same calcination conditions (700 °C, 3 h). It can be observed from Figure 6 that as the CN-CA molar ratio changes from 1/0.5 to 1/1.5, the intensities of the stretching vibration peaks of –OH (3648 cm^{-1}, 3448 cm^{-1}, and 1647 cm^{-1}) and CO_3^{2-} (1459 cm^{-1}, 871 cm^{-1} and 713 cm^{-1}) from CaO(S) are reduced respectively [42,43], which was attributed to the formation of calcium citrate complexes between CA and Ca^{2+}, avoiding the precipitation of Ca^{2+} and promoting the hydrolysis and polycondensation of calcium salts, indicating that with the increase of the amount of CA, the surface of CaO(S) is less eroded by CO_2 and H_2O in the air.

3.1.5. *CO_2-TPD analysis*

The CO_2-TPD curves of CaO(S) were measured by temperature-programmed desorption by using CO_2 as the acid probe molecule. Its results are shown in Figure 7(a,b) and the total basicity is presented in Table 3. It can be seen from Figure 7(a) that all the peaks of the CO_2-TPD curves of CaO(S) appear in the high temperature region (600–800 °C), which is a strong chemical adsorption site, indicating that CaO(S) belongs to a strong solid base. When the calcination temperature is 600 °C, the crystal phase of 1/1-CaO(S)-600 is carbonate with

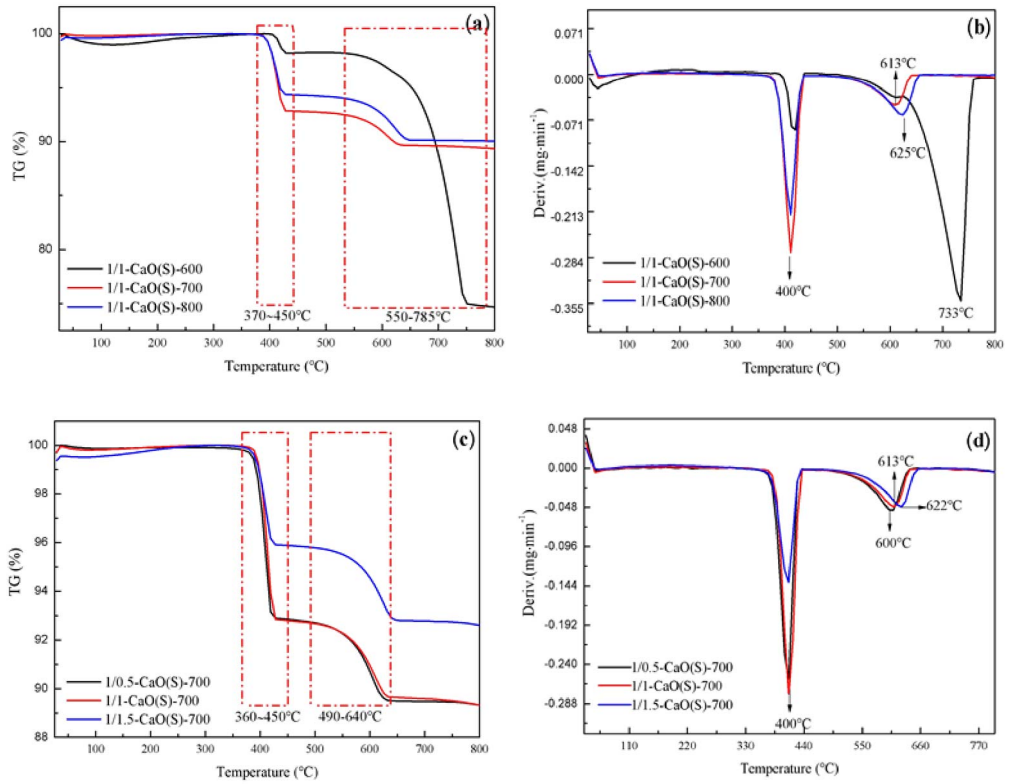

Figure 5. TG-DTA curves of the synthesized CaO(S) (a,b) calcination conditions; (c,d) the mole ratio of nitrate and citric acid.

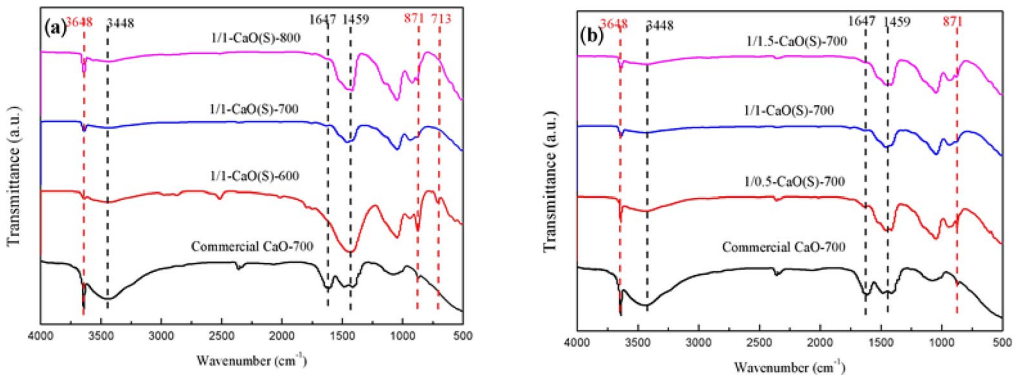

Figure 6. FT-IR spectras of the synthesized CaO(S) and Commercial CaO-700 (a) calcination conditions; (b) the mole ratio of nitrate and citric acid.

rhombohedral structure. When the calcination temperature is changed from 600 °C to 700 °C, the pyrolysis of CaO(S) gel is more sufficient, and the active CaO grains gradually nucleate and grow so as to the total basicity is 5.90 mmol/g. However, the reduced total basicity (3.89 mmol/g) exhibited by 1/1-CaO(S)-800 is due to the sintering of its surface, which reduces the specific surface area.

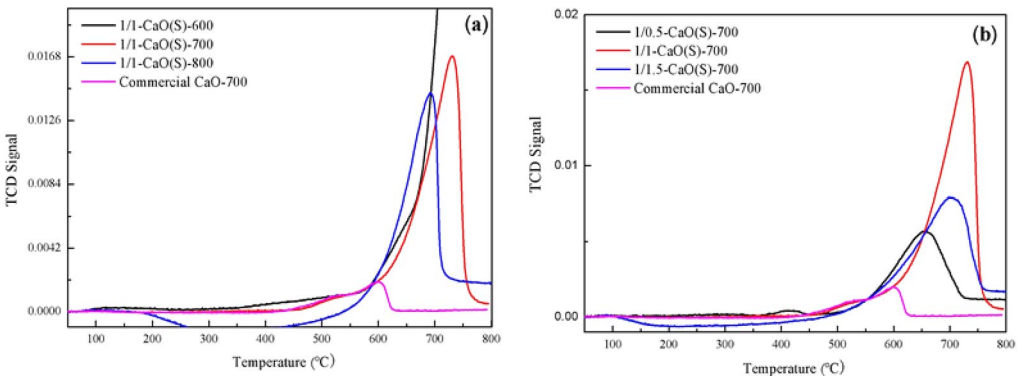

Figure 7. CO_2-TPD curves of the synthesized CaO(S) and Commercial CaO-700 (a) calcination conditions; (b) the mole ratio of nitrate and citric acid.

As presented in Figure 7(b), when the CN-CA molar ratio increases from 1/0.5 to 1/1, the CO_2 desorption peak area of CaO(S) becomes larger, and the total basicity increases in range of 2.10–5.90 mmol/g. The 1/1.5-CaO(S)-700 produced by the CN-CA molar ratio of 1/1.5 has a decreased total basicity (3.21 mmol/g), which is due to the increase of CA improves the stability of CaO(S) gel and deteriorates the dispersion of CaO particles.

3.1.6. *SEM analysis*

Figure 8 shows the SEM images of the pollen before and after ethanol ultrasonic treatment (a,b), CaO(S) (c–e) prepared at different calcination temperatures and Commercial CaO-700 (f). It can be seen from Figure 8 that when the calcination temperature is 600 °C, the CaO(S) prepared by the sol–gel method can still see the embryonic form of the pollen, and its particle size distribution is in range of 0.47–0.85 μm [44]. When the calcination temperature is 700 °C, the particles of CaO(S) are more uniformly dispersed, and the particle size distribution is presented by 0.11–0.26 μm. However, a calcination temperature of 800 °C can trigger the sintering and agglomeration of the CaO(S) surface, and the particle size distribution is 0.37–0.68 μm.

3.2. *Catalytic performance of the CaO(S) catalysts*

The catalytic activity of CaO(S) derived from different calcination temperatures was investigated at 65 °C, n(oil/methyl acetate/methanol) = 1/1/8, and CaO(S) dosage = 10 wt%. It can be seen from Figure 9(a) that when the calcination temperature is 600 °C, 700 °C and 800 °C, respectively, the yields of CaO(S) catalyzed transesterification to FAME can reach 3.45%, 96.62% and 64.99%, the reaction times are 3.5 h, 3 h, and 3 h, indicating that an increase in the calcination temperature from 600 °C to 700 °C is advantageous to increase the reaction rate of transesterification and shorten the reaction time, which is related to its increased specific surface area [45].

Based on the results of Figure 9(a), the effects of different CN-CA molar ratios on the catalytic activity of CaO(S) at 700 °C calcinating is described at 65 °C, n(oil/methyl acetate/methanol) = 1/1/8, CaO(S) dosage = 10 wt%, as shown in Figure 9(b). It can be seen from Figure 9(b) that when the CN-CA molar ratio is 1/0.5, 1/1 and 1/1.5, the FAMEs produced by the corresponding 1/0.5-CaO(S)-700, 1/1-CaO(S)-700 and 1/1.5-CaO(S)-700 can reach the highest in 3 h, which are 89.61%, 96.62% and 92.38%. There is an explanation confirmed that appropriately changing the ratio of CN-CA can increase the reaction rate of transesterification, which is attributed to the fact that citric acid easily forms a complex with Ca^{2+} in ethanol solution, and the CaO(S) gel becomes stable [46].

The relationship between different doses of 1/1-CaO(S)-700 and FAME yield at 65 °C, n(oil/ester/alcohol) = 1/1/8 is presented in Figure 10(a). From Figure 10(b), a trend of increasing FAME yield of 1/1-CaO(S)-700 with dosage ranging from 5 wt% to 10 wt% was observed over time within 3 h of transesterification. Specifically, when the

Table 3. Total basicity of CaO(S) and Commercial CaO-700

Type of catalyst	Total basicity (mmol/g)	Desorption peaks (area%)
1/1-CaO(S)-600	-	-
1/1-CaO(S)-700	5.90	1.37
1/1-CaO(S)-800	3.89	0.90
1/0.5-CaO(S)-700	2.10	0.49
1/1.5-CaO(S)-700	3.21	0.75
Commercial CaO-700	0.79	0.18

dosage of 1/1-CaO(S)-700 is 5 wt% and 10 wt%, the yield of FAME within 3 h is 73.07% and 96.62%. Extending the reaction time to 3.5 h, the FAME yield of 1/1-CaO(S)-700 at 5 wt% still increase slowly, to 74.90%, while the FAME yield of 1/1-CaO(S)-700 at 10 wt% decrease slightly, to 92.63%, which suggests that increasing the amount of 1/1-CaO(S)-700 is conducive to providing more basic sites, thus increasing the reaction rate and enhancing the catalytic effect. However, the generation of unfavorable reactions (saponification reaction) would reduce the transesterification effect with the participation of 1/1-CaO(S)-700 (15 wt%), which reduced the FAME yield to 78.81% at 3 h [47].

The effect of the reaction temperature of 1/1-CaO(S)-700 on the FAME yield at CaO(S) dosage = 10 wt%, n(oil/ester/alcohol) = 1/1/8 was investigated, as shown in Figure 10(b). It is available from Figure 10(b) that in the presence of 1/1-CaO(S)-700, the FAME yields within 3 h at 60 °C, 65 °C and 70 °C are 49.52%, 96.62% and 81.19%. Subsequently, when the reaction time is extended to 3.5 h, the FAME yield increased to 61.32% at 60 °C, while the FAME yields decrease slightly at 65 °C and 70 °C, as presented by 92.62% and 79.11%, which indicates that an increase of the reaction temperature by 1/1-CaO(S)-700 is favourable to encourage the transesterification reaction (endothermic reaction). When the reaction temperature of 1/1-CaO(S)-700 continues to 70 °C, the volatilization of low-boiling methanol is induced [48].

The carbon chain length, steric effect and dosage of lower alcohols have important influence on the transesterification reaction. Methanol, as one of the alcohols with the shortest carbon chain and the smallest steric resistance, has the strongest nucleophilicity. Therefore, the effect of methanol dosage on FAME yield was examined at 65 °C, $1/1-CaO(S)$-700 dosage = 10 wt%, and the results are shown in Figure 10(c). It can be seen from Figure 10(c) that when n(oil/ester/alcohol) is 1/1/6, 1/1/8, and 1/1/10, the FAME yields within 3 h reach 71.70%, 96.62%, 6.64%, respectively, which is due to the dilution of the system caused by excess methanol molecules [49]. Methyl acetate added in the reaction can directly react with the resulting glycerol, achieving online conversion of glycerol at the stoichiometric ratio of 1/1. The amount of methanol was investigated in detail due to it is a great important factor to improve the reaction to shift to the right, thereby improving the conversion rate of oil [50].

Moreover, the 1/1-CaO(S)-700 from the reacted mixture can be regenerated by centrifugation and washing with ethanol and calcination of 700 °C in order to remove the oil and glial molecules inside the catalyst. After regeneration, the cyclic catalytic ability of 1/1-CaO(S)-700 and commercial CaO-700 was explored under optimal conditions, as shown in Figure 11(a). It can been seen that the yields of FAME catalyzed by 1/1-CaO(S)-700 are 96.62%, 95.40% and 91.37%, all of which remains above 90% in 3 cycles, and the excellent recyclability of 1/1-CaO(S)-700 indicates its good catalytic stability under transesterification reaction. In commercial CaO, the FAME yield maintains on a relatively low level after reused in three cycles, no more than 56%. Furthermore, it can been found that 1/1-CaO(S)-700 prepared by sol–gel method showed stable catalytic activity than commercial CaO, as implied by Figure 11(b). Some properties of prepared biodiesel produced by CaO(S) including relative density, viscosity, flash point, ester content and free glycerol are listed in Table 4. It can be seen that the various performance indicators

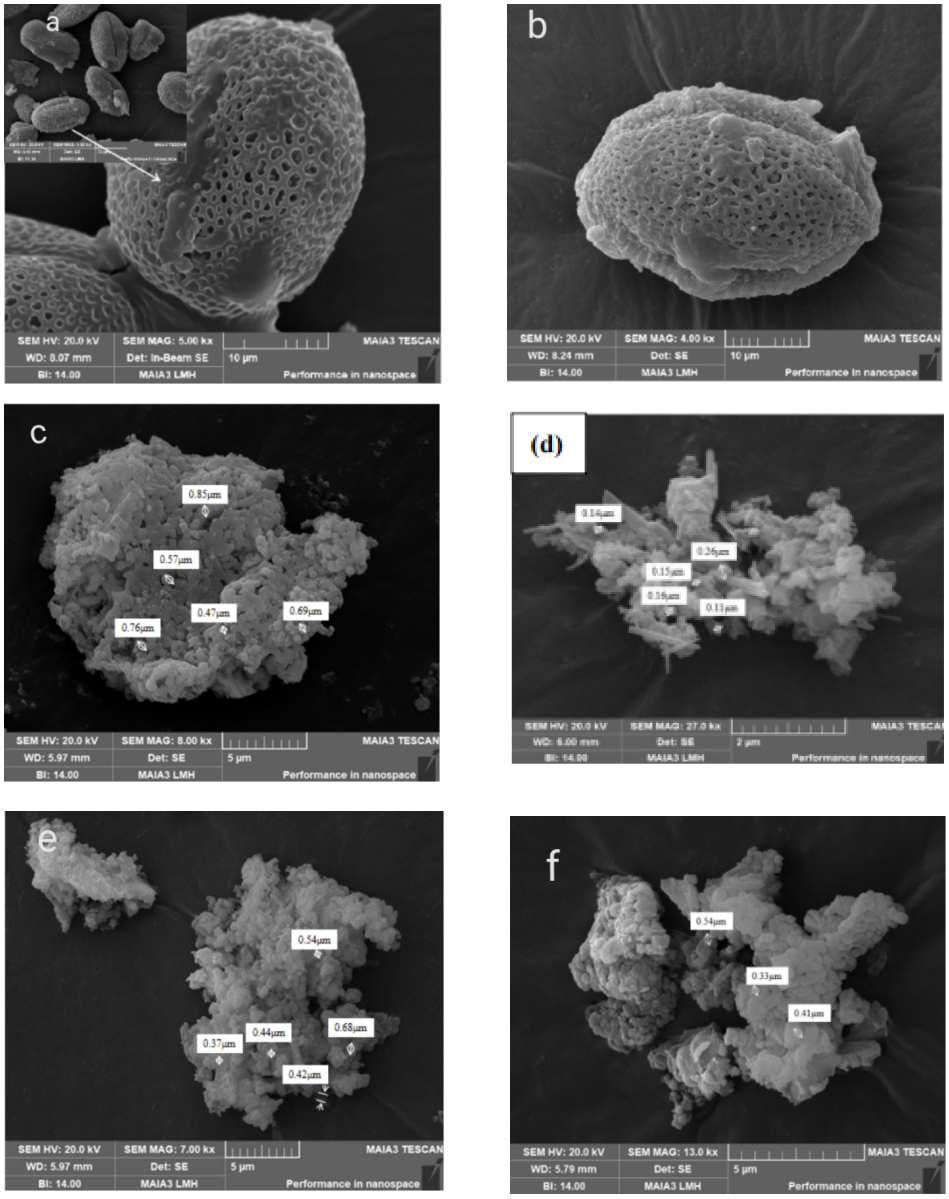

Figure 8. SEM of CaO(S) under different calcination conditions (a) original pollen (b) pretreated pollen (c) 1/1-CaO(S)-600 (d) 1/1-CaO(S)-700 (e) 1/1-CaO(S)-800 (f) Commercial CaO-7.

of the biodiesel meet the European biodiesel standards [51]. Furthermore, it is evident that the main resource of obtained CaO(S) is derived from commercial CaO which has brought important benefits for industrial applications due to its excellent basicity [52] and low cost at approximately $2.9/kg compared with the value of KOH, at approximately $3.3/kg.

4. Conclusions

In summary, series of CaO(S) materials were prepared based on a combination of pollen and sol–gel method via solvation, alcohololysis, condensation, followed by the calcination decomposition. Compared with commercial CaO calcinated at 700 °C, as-prepared 1/1-CaO(S)-700 possesses larger BET

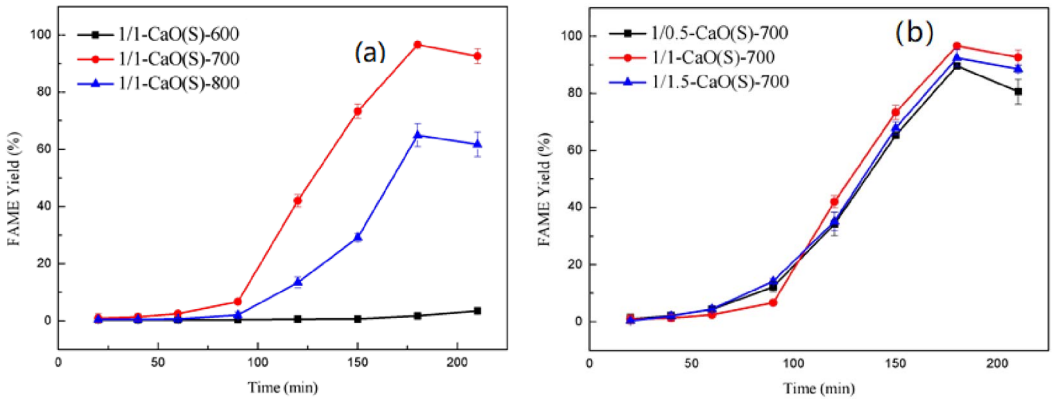

Figure 9. Catalytic activity of CaO(S) under different (a) calcination condition; (b) mole ratio of calcium nitrate and citric acid.

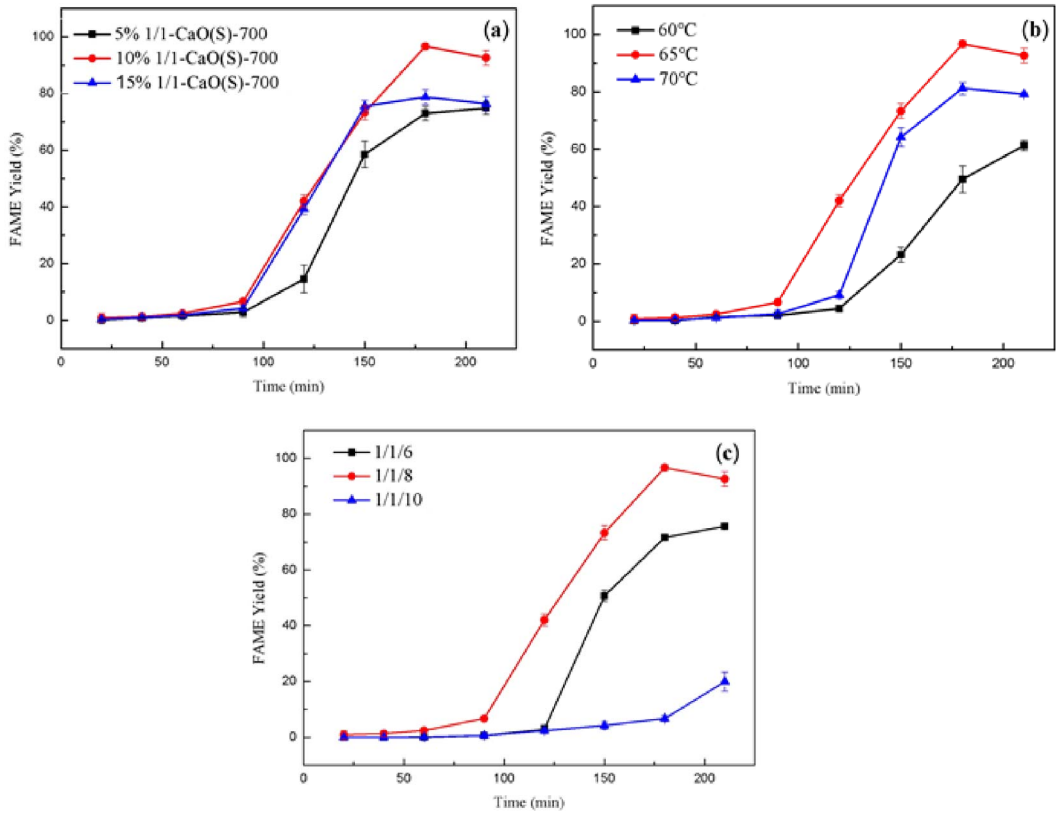

Figure 10. Effect of reaction parameters of CaO(S) on FAME yield (a) the catalyst amount (b) the reaction temperature (c) the oil/ester/alcohol ratio.

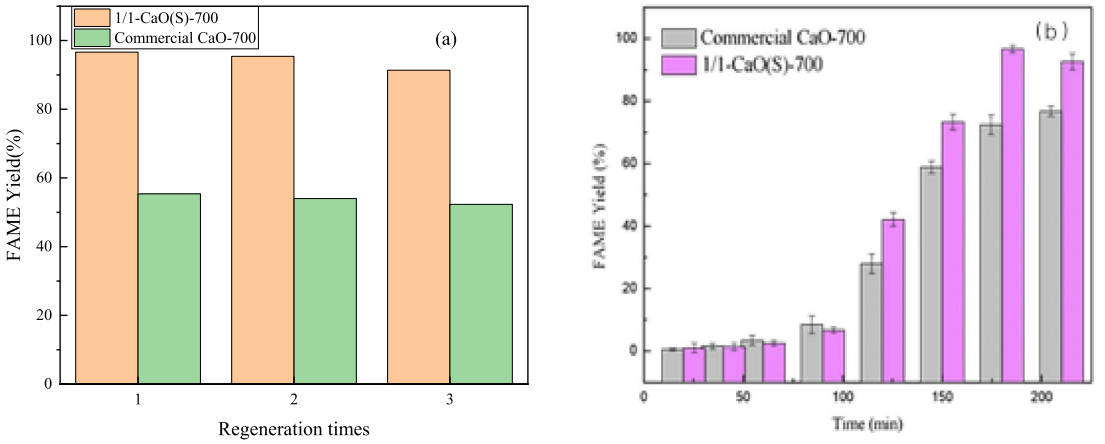

Figure 11. (a) Regeneration analysise of 1/1-CaO(S)-700 and Commercial CaO-700 in transesterification; (b) Catalytic activity of commercial CaO-700 and CaO(S).

Table 4. Fuel properties of biodiesel

Properties	Test method	EN14214
Relative density, 298 K	0.89	0.86–0.90
Viscosity, 313 K (mm^2/s)	4.6	3.5–5.0
Flashpoint (K)	437	>373
Ester content (%)	91.8–99.8	96.5
Free glycerol (%, m/m)	0.018	<0.02

surface areas of 16.4746 m^2/g, hierarchical structure with pore size distribution of 2–12.5 nm, total basicity of 5.9018 mmol/g and strong basic sites (CO_2-desorption temperature around 700 °C), thereby promoting the diffusion of reactants in heterogeneous reaction systems and improving their reaction efficiency. Consequentially, the resulting 1/1-CaO(S)-700 is predicted considerable activity in the transesterification reaction of oil-methyl acetate-methanol. The yield of biodiesel catalyzed by 1/1-CaO(S)-700 via diffusing or depositing of Ca^{2+} in confined spaceas (pollen) by the sol–gel approach is obviously higher than that by commercial CaO, as presented by 96.62% after 3 h under 65 °C, the dosage of 1/1-CaO(S)-700 of 10 wt%, oil/methyl acetate/methanol of 1/1/8. Furthermore, its regeneration performance shows that 1/1-CaO(S)-700 has significant catalytic stability with the yield of 91.37% after 3 cycles. This study provides a facile and efficient synthetic path for calcium oxide with hierarchical structure and improves total basicity, opening up more opportunities for its application in biodiesel production or other organic reactions involving calcium oxide.

Declaration of interests

The authors do not work for, advise, own shares in, or receive funds from any organization that could benefit from this article, and have declared no affiliations other than their research organizations.

Funding

The work was supported financially by the National Natural Science Foundation of China (51974252), the Youth Innovation Team of Shaanxi University and Xi'an Shiyou University Graduate Innovation Project (YCS22213106).

Acknowledgments

We thank the work of Modern Analysis and Testing Center of Xi'an Shiyou University.

References

[1] M. H. Rahman, A. Ruma, M. N. Hossain *et al.*, *Int. J. Energy Econ. Policy*, 2021, **11**, 121-129.
[2] N. Zhang, L. Miao, *IOP Conf. Ser. Earth Environ. Sci.*, 2021, **668**, article no. 012025.

[3] A. Demirbas, K. Al-Ghamdi, N. Sen *et al.*, *Petr. Sci. Technol.*, 2017, **38**, 1-7.
[4] M. S. Rana, A. Al-Barood, R. Brouresli *et al.*, *Fuel Process. Technol.*, 2018, **177**, 170-178.
[5] Y. C. Huang, Y. T. Li, K. Luo *et al.*, *Proc. Inst. Mech. Eng. D*, 2020, **234**, article no. 095440702091698.
[6] N. Zik, S. Sulaiman, P. Jamal *et al.*, *Renew. Energy*, 2020, **155**, 267-277.
[7] C. Decarpigny, A. Aljawish, C. His *et al.*, *Energies*, 2022, **15**, article no. 3381.
[8] S. D. Manali, C. B. Scott, D. Y. Ganapati *et al.*, *Catalysis Today*, 2020, **375**, 101-111.
[9] H. Mazaheri, H. C. Ong, Z. Amini *et al.*, *Energies*, 2021, **14**, 3950-3973.
[10] D. M. Marinković, M. V. Stanković, A. V. Veličković *et al.*, *Renew. Sustain. Energy Rev.*, 2016, **56**, 1387-1408.
[11] J. Wang, T. L. Yan, Y. Tang *et al.*, *Kinetics Catal.*, 2016, **57**, 439-445.
[12] F. Simanjuntak, T. K. Kim, D. L. Sang *et al.*, *Appl. Catal. A: General*, 2011, **401**, 220-225.
[13] M. C. Leandro, M. A. S. Rosana, D. S. C. Natália *et al.*, *Bioresour. Technol.*, 2014, **151**, 207-213.
[14] B. Qiu, Y. Mao, X. Xiao *et al.*, *Solar Energy*, 2021, **220**, 63-69.
[15] F. Hadi, K. Omid, N. Firouzeh *et al.*, *Synthetic Metals*, 2016, **215**, 142-149.
[16] Z. H. Li, J. C. Ouyang, G. Q. Luo *et al.*, *Ind. Eng. Chem. Res.*, 2019, **58**, 22040-22047.
[17] Z. Y. Zhao, H. M. Chen, N. Wang *et al.*, *Rare Metal Mater. Eng.*, 2013, **42**, 2467-2471.
[18] T. C. Wang, Q. K. Yu, J. Kong *et al.*, *Int. J. Appl. Ceramic Technol.*, 2018, **15**, 472-478.
[19] Y. Liu, X. D. Zhu, D. L. Yuan *et al.*, *Sci. Rep.*, 2020, **10**, article no. 12444.
[20] H. Y. Sun, *Int. J. Electrochem. Sci.*, 2018, **13**, 4753-4762.
[21] B. Abarna, T. Preethi, A. Karunanithi *et al.*, *Mater. Sci. Semiconductor Process.*, 2016, **56**, 243-250.
[22] S. Zhao, L. Wang, Y. Wang *et al.*, *J. Phys. Chem. Solids*, 2018, **116**, 43-49.
[23] S. Tao, Z. Li, F. L. Qin *et al.*, *C. R. Chim.*, 2022, **25**, 145-153.
[24] P. Phatai, C. M. Futalan, S. Kamonwannasit *et al.*, *J. Sol–Gel Sci. Technol.*, 2019, **89**, 764-775.
[25] B. Jiang, X. W. Cha, Z. L. Huang *et al.*, *Mol. Catal.*, 2022, **524**, 112251-112286.
[26] M. J. Uddin, S. Liyanage, N. Abidi *et al.*, *J. Pharm. Sci.*, 2018, **107**, 3047-3059.
[27] Y. Yang, H. Liu, J. Zhang *et al.*, *Inorg. Nano-MetChem.*, 2022, **52**, 1030-1040.
[28] Y. Tang, Z. Y. Li, Z. Y. Xu *et al.*, *RSC Adv.*, 2020, **10**, 28695-28704.
[29] M. Hayati-Ashtiani, *Particle Particle Syst. Character.*, 2012, **28**, 71-76.
[30] A. Hemalatha, S. Arulmani, E. Chinnasamy *et al.*, *Mater. Today: Proceed.*, 2020, **34**, 412-415.
[31] Y. Tang, Y. Yang, H. Liu *et al.*, *Inorg. Nano-Met. Chem.*, 2020, **50**, 501-507.
[32] S. V. Berzin, K. A. Dugushkina, M. V. Chervyakovskaya *et al.*, *Lithosphere (Russia)*, 2021, **21**, 409-430.
[33] Z. Y. Li, Z. F. Zhang, Y. B. Lian *et al.*, *Indian J. Biochem. Biophys.*, 2021, **58**, 457-463.
[34] M. A. Maximov, A. V. Galukhin, G. Y. Gor *et al.*, *Langmuir*, 2019, **35**, 14975-14982.
[35] J. Wang, S. Tao, Y. F. Zhao *et al.*, *J. Biobased Mater. Bioenergy*, 2021, **15**, 296-301.
[36] A. Nunes, F. Castilhos, *Fuel*, 2020, **267**, article no. 117264.
[37] Y. Tang, T. L. Yan, B. Shen *et al.*, *Can. J. Chem. Eng.*, 2016, **94**, 1466-1471.
[38] Q. T. Tien, G. Q. Guan, G. G. Liu *et al.*, *Monatshe. für Chem. Chem. Month.*, 2017, **148**, 1235-1243.
[39] Y. Yang, S. Tao, G. T. Li *et al.*, *Int. J. Chem. Kinet.*, 2024, **56**, 20-29.
[40] S. Tao, Z. F. Zhang, M. Meng *et al.*, *Theor. Exp. Chem.*, 2021, **57**, 378-385.
[41] C. Huang, S. Bai, J. Lv *et al.*, *Catal. Lett.*, 2011, **141**, 1391-1398.
[42] A. Knk, B. Sns, C. Csak *et al.*, *Renew. Energy*, 2020, **146**, 280-296.
[43] W. W. Mar, E. Somsook, *Scienceasia*, 2012, **38**, 90-94.
[44] W. Shen, L. Zhang, Y. Du *et al.*, *Mater. Lett.*, 2018, **213**, 7-10.
[45] Y. Tang, Y. Yang, H. Liu *et al.*, *J. Chem. Technol. Biotechnol.*, 2020, **95**, 1467-1475.
[46] K. S. Ravi, K. Deepak, G. Ranjana, *Ceramics Int.*, 2016, **42**, 4090-4098.
[47] Y. Tang, Q. T. Cheng, H. Cao *et al.*, *C. R. Chim.*, 2015, **18**, 1328-1334.
[48] Y. Tang, H. Liu, Z. Y. Li *et al.*, *J. Chem. Technol. Biotechnol.*, 2020, **95**, 1234-1242.
[49] R. Estevez, C. Luna, J. Calero *et al.*, *Mol. Catal.*, 2020, **484**, article no. 110804.
[50] S. Saka, Y. Isayama, *Fuel*, 2009, **88**, 1307-1313.
[51] Y. Tang, J. Xu, J. Zhang *et al.*, *J. Cleaner Product.*, 2013, **42**, 198-203.
[52] M. López Granados, D. Martín Alonso, A. C. Alba-Rubio *et al.*, *Energy Fuels*, 2009, **23**, 2259-2263.